Regular Article

Band structure and transmission spectra in multiferroic based Sierpinski-carpet phononic crystal[★]

Zafer Ozer[1,*], Selami Palaz[2], Amirullah M. Mamedov[3,4], and Ekmel Ozbay[3]

[1] Mersin Vocational High School Electronic and Automation Department, Mersin University, Mersin, Turkey
[2] Faculty of Science, Department of Physics, Haran University, Sanliurfa, Turkey
[3] Nanotechnology Research Center (NANOTAM), Bilkent University, Ankara, Turkey
[4] International Scientific Center, Baku State University, Baku, Azerbaijan

Abstract. In this study, the band structure and transmission spectra in multiferroic based Sierpinski-carpet phononic crystal are investigated based on finite element simulation. In order to obtain the band structure of the phononic crystal (PnC), the Floquet periodicity conditions were applied to the sides of unit cell. The square lattice PnC consists of various piezoelectric inclusion in a rubber matrix with circular and triangular cross section.

1 Introduction

Metamaterials opened new opportunities for controlling radiation. Acoustic metamaterials (AMs) and phononic crystals (PnCs) are drastically different from the constituents of the traditional and other left-handed materials. A number of AM-based conceptual functionalities have been designed and realized experimentally in the last decade [1–3]. Due to the having many promising applications and unique physical properties, PnCs have become great interest recently [4–6]. The presence of band gaps (BGs) where non-propagating modes may occur in the system leads to a variety of potential applications such as, waveguides, sound filters, noise and vibration reduction [7–11]. Due to the potential applications of PnC designs with wide BG structure and adjustable bands in communication, mechanical and control engineering, the researchers concentrated their work [12–15].

Many researchers have recently focused on fractal structures to investigate its effect on band structure [2,3,16–25].

Fractal designs are an innovative approach for researchers working on photonic crystals and multimodal plasmonic devices [17–19]. Studies on dispersion properties of fractal structures in different geometries were carried out. [20–25]. In present investigation we would like demonstrate a new kind of acoustic metamaterial element with fractal geometry, which is inspired by the fractal

features of geography in the natural world [26,27]. Fractal acoustic metamaterial (FAM) is a tapered structure with self-similar mathematical description [27]. Although they may appear complex, FAMs can be easily designed to obtain specific parameters through high resolution computer programs and can be reliably fabricated with existing rapid-prototyping technology. Fractal surfaces have such properties, like sound scattering by a fractal surfaces. One of these fractal designs, the Sierpinski-carpet, was described in 1916 by Waclaw Sierpinski [27]. The Sierpinski carpet will have the aforementioned properties if its inhomogeneities of sequentially decreasing scale have alternative signs. Geometrically, the construction of the Sierpinski carpet is as follows. An initial square is divided by two lines parallel to one pair of its sides and by two lines perpendicular to them into nine equal squares of smaller size. The central square is separated from them. Another eight squares are divided in the same way into nine squares of smaller scale, and the central squares are separated from them, and so on. A fractal structure is formed in the limit. In this structure, each separated square of a given linear dimension is surrounded by eight separate squares of a thrice smaller linear dimension. In reality, the subdivision of squares ends at a certain step n. The acoustic Sierpinski carpet is a set of inhomogeneities in the form of squares with sequentially decreasing side lengths H_n ("a"), n = 0, 1, 2, ..., where $H_n = 3^{-n}H$ and H is the side of the central square. The number of squares of the n-th scale is equal to 8^n, and the total area of the squares of this scale is $8^n H_n^2 = H^2(8/9)^n$. From this formula, it follows that the total area of the squares of the n-th scale slowly decreases with the growth of n and is equal to eight-ninths of the area of the preceding scale.

In this study, firstly, the quasi-Sierpinski-carpet phononic crystal unit cell was identified and then the

---

[★] Contribution to the Topical Issue "Advanced Electromagnetic Materials and Devices (META 2019)", edited by A. Razek and S. Zouhdi.
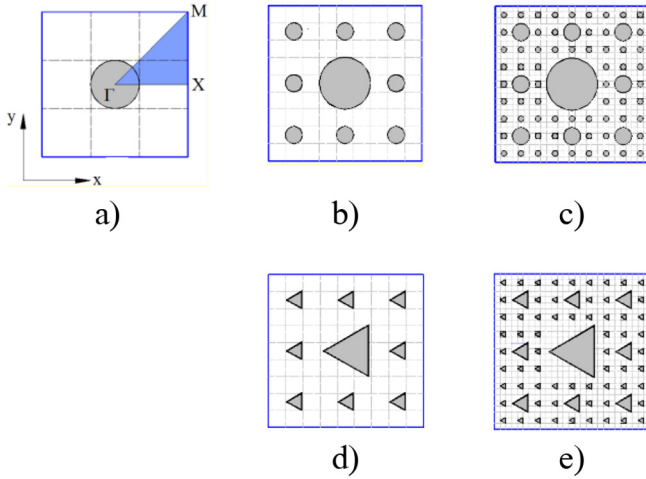
* e-mail: zaferozer@mersin.edu.tr

Fig. 1. Traditional Sierpinski-carpet unit cells at different levels with circular cross-section (a) *L1*; (b) *L2*; (c) *L3* levels with triangular cross-section (d) *L2*; (e) *L3* levels.

Table 1. Material properties.

Material	BaTiO$_3$	LiNbO$_3$
ρ [kg/m^3]	6020	4700
d$_{31}$ [m/V]	-3.45E-11	-1.00E-12
d$_{33}$ [m/V]	8.56E-11	6.00E-12
d$_{15}$ [m/V]	3.92E-10	6.80E-11
s$^E_{11}$ [m.s^2/kg]	8.05E-12	5.78E-12
s$^E_{33}$ [m.s^2/kg]	1.57E-11	5.02E-12
s$^E_{12}$ [m.s^2/kg]	-2.35E-12	-1.01E-12
s$^E_{13}$ [m.s^2/kg]	-5.24E-12	-1.47E-12
s$^E_{44}$ [m.s^2/kg]	1.84E-11	1.70E-11
s$^E_{66}$ [m.s^2/kg]	8.84E-12	1.36E-11
$\varepsilon^S_{11}/\varepsilon_o$	2920	84
$\varepsilon^S_{11}/\varepsilon_o$	168	30

band structure was obtained along Γ-X-M-Γ the path. Figure 1 shows the unit cells of different filling fractions and cross-sections of traditional Sierpinski-carpet phononic crystals.

2 Method

In order to obtain the band structure of the PnC, the Floquet periodicity conditions were applied to the sides of unit cells 1–4 and 2–3 in Figure 1a. The square lattice PnC consists of BaTiO$_3$ and LiNbO$_3$ inclusion in a rubber matrix with circular and triangular cross section.

In our case, the traditional Sierpinski-carpet producing procedure begins with a square of length "*a*" is divided into 9 identical subsquares in the 3-by-3 grids and the central subsquare is subtracted and filled with piezoelectric inclusion to form the first step (*L1*). Then, the same procedure is applied repeatedly to the remaining 8 sub-squares (*L2*). With this method, fractal structures of different levels could be formed up to last in different geometries.

In PnC's, some arrangements are made on the Sierpinski-carpet to increase the filling fraction, which is an important feature affecting the band structure. For each step, the first frame is taken as a reference (Fig. 1a), the unit cell is subdivided into sub-squares with the grids o obtain the supercell as shown in Figures 1b and 1c.

In Figure 1, by applying to the Floquet periodicity conditions to the edges of the super cell the band structures are obtained using the finite element method (FEM). In the Sierpinski-carpet fractal production procedure at different levels of the reference cross-sections (circle and triangle) was used in Figure 1a. With the formula $n = m^{2L}$, the number of grids in the center of the unit cell for $L = i$ ($i = 2,3$) was obtained according to this production procedure. In this fractal production procedure, m is the number of grids in step x and y in step 1, and k is the number
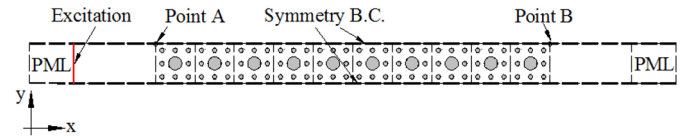

Fig. 2. Used finite array for obtaining the transmission spectra of PnC.

of sub-squares in direction x or y in the first step. The mechanical properties of the rubber matrix are obtained from literature [24]. The piezoelectric material properties in the rubber matrix used in analysis are as shown in Table 1 [28].

We used the finite array of scatterers in Figure 2 for calculating the transmission spectra of PnC. The transmission spectra were calculated according to absolute displacement as in literature 20log10(U$_B$/U$_A$) in dB where U$_A$ and U$_B$ are normalized displacement at A and B point respectively [29–32].

3 Results and discussions

We used circular and triangular cross-section rods as seen in Figure 1 in circular lattice Sierpinski-carpet fractals with three levels (*L1*, *L2* and *L3*) of PnC.

While there was no band observed in any triangular cross-section and any inclusion material in case of traditional Sierpinski-carpet *L1*, *L2* and *L3* levels. In case of circular cross-section with BaTiO$_3$ inclusion in case *L1* level only 1 band observed 2.78 gap size at 2.08 frequency and 2.39 gap size at 2.1 frequency in case of LiNbO$_3$ inclusion. In case of *L2* level when BaTiO$_3$ circular cross-section rods used, we observed 0.17 gap size at 2.27 frequency and 0.04 gap size at 2.12 frequency in case of LiNbO$_3$ inclusion. There were band observed in circular cross-section BaTiO$_3$ and LiNbO$_3$ inclusions in case of *L3* level.

In quasi Sierpinski-carpet where there was $K = 4$, and $M = 6$ *L1* level, there was a wide full band observed at a
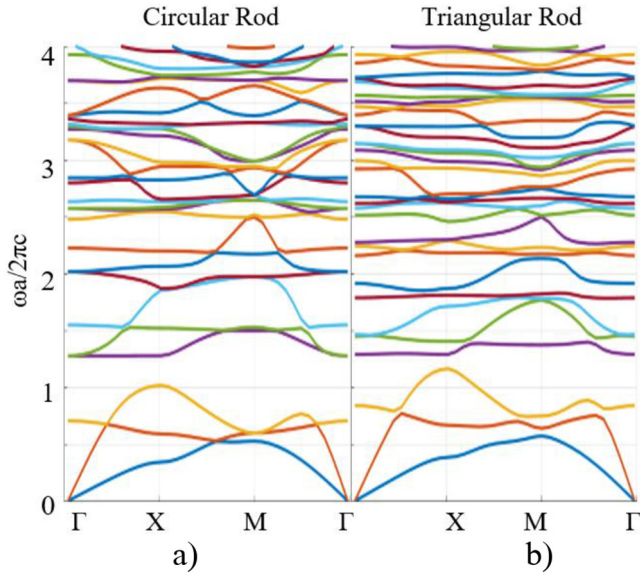
Fig. 3. Band structure of quasi-Sierpinski carpet PnC consists of $BaTiO_3$ in a rubber matrix in case K4, M6, L1 (a) circular rod; (b) triangular rod.
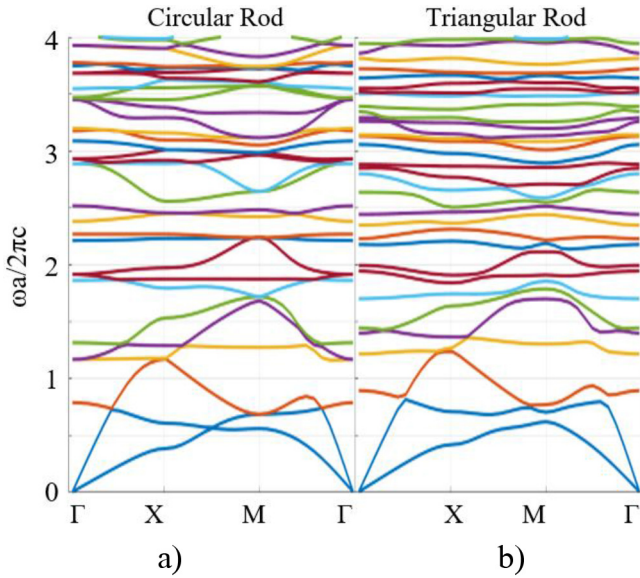

Fig. 4. Band structure of quasi-Sierpinski carpet PnC consists of $BaTiO_3$ in a rubber matrix in case K4, M6, L2 (a) circular rod; (b) triangular rod.
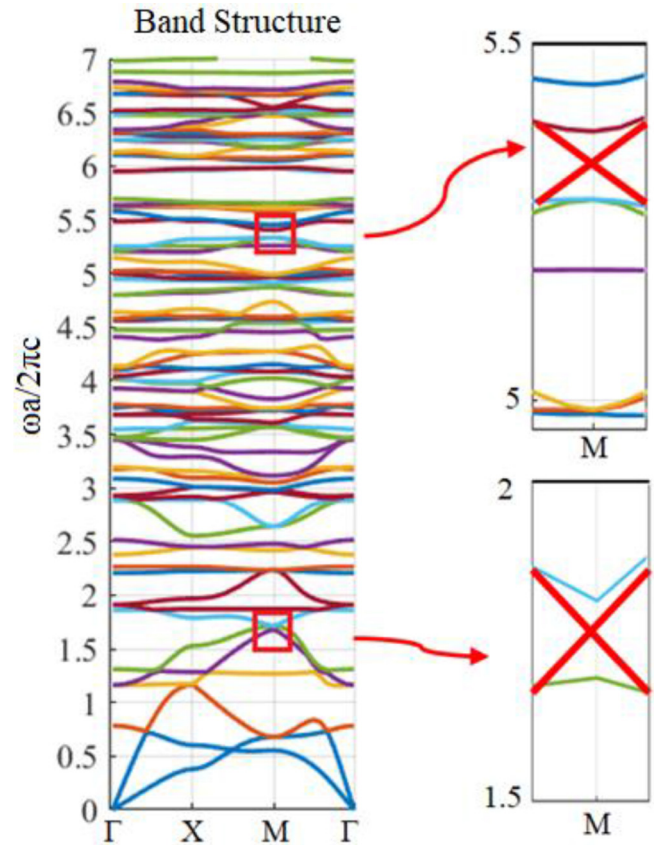

Fig. 5. Band structure of $BaTiO_3$/rubber PnC and topological insulator properties in case M6K4 L2.

cross-section inclusion. It could be said that $BaTiO_3$ based PnC has a topological phase as in some narrow-band insulators. The band structure includes Dirac point degeneration, which is characterized by the presence of the circulating medium. The resulting acoustic bands have non-zero numbers indicating that they are topologically nontrivial [33].

Figure 6 shows the 3D band structure of $BaTiO_3$/ rubber PnC for first three modes with their associated reduced velocities along the Γ-X-M-Γ direction in *M6K4L2* case.

We have created a new quasi-Sierpinski-carpet fractal design that combines the central circle with sub-circles based on the *M6K4L2* design shown in Figure 7. We obtained the band structure and transmission spectra of new fractal by using $BaTiO_3$/$LiNbO_3$ inclusions in the rubber matrix. Figure 8 shows band structure and transmission spectra of $BaTiO_3$/rubber and $LiNbO_3$/ rubber PnC's respectively. As seen Figure 8 the new fractal structure has the wide BG.

We obtained the transmission spectra of PnC by using the finite array in Figure 2 and compared them with the band structure of case *M6K4*. Figure 9 shows a comparison of the band structure and transmission spectra for all of investigated types scatterers.

As seen in Figure 9a BG's observed between 2.27 and 2.38 as well as 2.52 and 2.58 for $BaTiO_3$/rubber PnC and between 2.45 and 2.50 for $LiNbO_3$/rubber PnC as seen in Figure 9b.
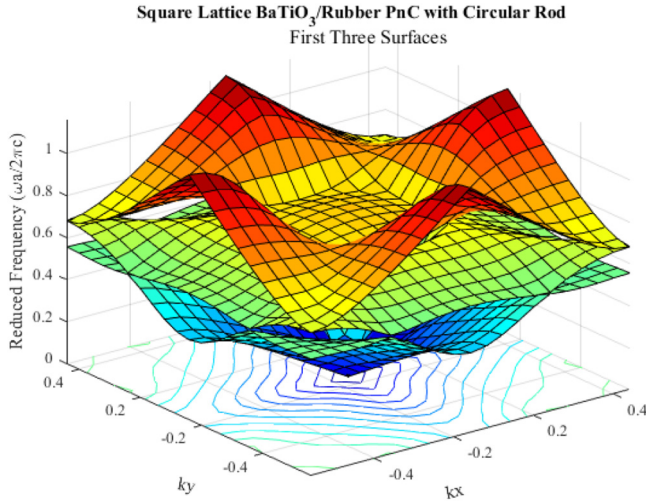
22.73 gap size at 1.15, 10.03 gap size at 1.23 frequencies for circular and triangular $BaTiO_3$ inclusions as seen in Figure 3.

In quasi Sierpinski-carpet with circular cross-section $BaTiO_3$/rubber PnC at *L2* level, the low-frequency bands observed at the *L1* level were disappeared, but high-frequency bands occurred at 4.87, 1.5 gap sizes at 2.32, 1.87, 1 and 1.1 gap sizes at and 2.33, 3.44, 3.74, 3.83 frequencies as seen in Figure 4.

Figure 5 shows the dispersion relation of $BaTiO_3$/ rubber PnC with *M6K4L2* level PnC with circular

Fig. 6. 3D Band structure of BaTiO$_3$/rubber PnC for first three bands.
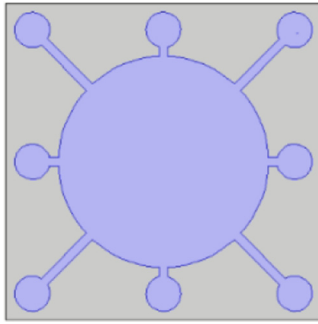

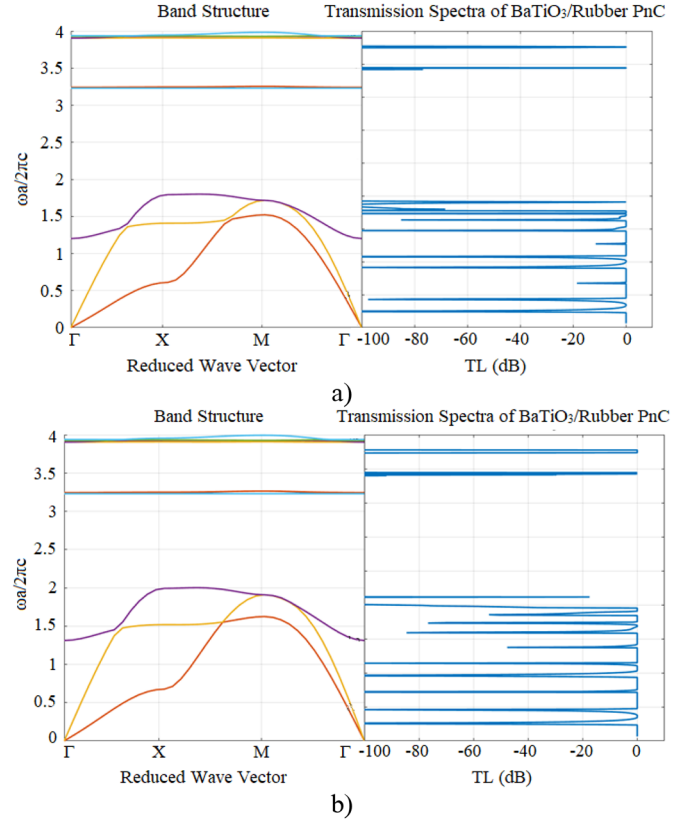**Fig. 7.** New quasi-Sierpinski-carpet fractal design based on M6K4 level 2.

Fig. 8. Band structure of circular cross-section scatterers (a) BaTiO$_3$; (b) LiNbO$_3$ in a rubber matrix M6K4 L2 level PnC and transmissions.

Table 2. Full band gap size variation of a quasi-Sierpinski-carpet case M6K4 Level 1 PnC with a circular and triangular cross-section.

Band Num.	Circular cross-section				Triangular cross-section			
	BaTiO$_3$		LiNbO$_3$		BaTiO$_3$		LiNbO$_3$	
	Mid Gap (a/c)	Gap Size (%)	Mid Gap (a/c)	Gap Size (%)	Mid Gap (a/c)	Gap Size (%)	Mid Gap (a/c)	Gap Size (%)
1	1.15	22.7	1.21	14.1	1.26	10.3	1.3	1.57
2	2.18	0.16	2.18	0.16	1.4	0.36	1.4	0.28
3	3.38	0.83	3.38	0.83	1.84	1.14	2.14	1.04
4	3.74	0.27	3.74	0.17	3.79	0.22	3.73	0.3
5	4.16	0.04	–	–	4.18	0.84	4.19	0.64
6	–	–	–	–	4.85	0.27	4.85	0.31

The band structures of quasi Sierpinski-carpet PnCs consisting of various BaTiO$_3$ and LiNbO$_3$ inclusions with circular and triangular cross-sections at *L1*, *L2* and *L3* levels are shown in Tables 2 and 3.

As can be seen from the tables while *L1* level PnC has a wide band range at low frequencies, has no multiband capability a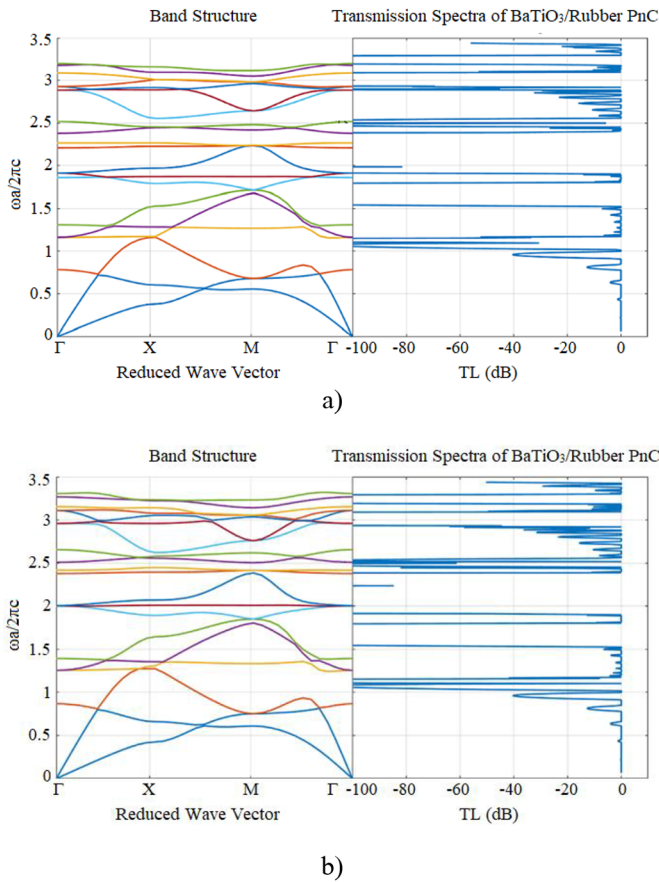nd *L2* and *L3* level PnCs have multiband characteristics at high frequencies, while the low frequency band disappears.

4 Conclusions

In this study, the band structure and transmission spectra in two dimensional 2D multiferroic based Sierpinski-carpet

Table 3. Full band gap size variation of a quasi-Sierpinski-carpet case M6K4 Level 2 PnC with a circular and triangular cross-section.

Band Num.	Circular cross-section				Triangular cross-section			
	BaTiO$_3$		LiNbO$_3$		BaTiO$_3$		LiNbO$_3$	
	Mid Gap (a/c)	Gap Size (%)	Mid Gap (a/c)	Gap Size (%)	Mid Gap (a/c)	Gap Size (%)	Mid Gap (a/c)	Gap Size (%)
1	2.32	4.87	2.48	2.25	2.12	1.07	2.21	1.24
2	2.53	1.5	3.64	0.8	2.32	1.46	2.32	1.34
3	4.35	1.33	4.53	1.62	3.45	1.87	3.95	1.56
4	4.77	1.32	5.84	3.97	4.74	1.46	4.28	0.74
5	5.17	1.33	6.96	1.51	5.90	1.24	5.94	0.82
6	5.82	4.4	7.17	0.43	6.60	1.33	6.64	0.79

Fig. 9. Band structure of circular cross-section scatterers (a) BaTiO$_3$; (b) LiNbO$_3$ in a rubber matrix M6K4 L2 level PnC and transmissions spectra's.

phononic crystal with circular and triangular cross-sections piezoelectric scatterers in a rubber matrix were investigated based on finite element simulation. We can summarize the results herein above:

– The broad band was observed at low frequency;
– The band structures are compatible with transmission spectra's;
– Inclusion geometry is effective on band structure;
– Better band structures can be achieved with different fractal designs;
– Proposed PnC has topological insulator properties;
– As seen from Figures 3 and 4, *L1* level PnC does not have multiband properties, although a multiband exists in *L2* levels. *L3* has difficulty in production and the width of the bands formed is narrower than *L2* level is not suitable for practical applications;
– As shown in [8] by applying voltage to the piezoelectric inclusions the proposed PnC can be used as actively guiding waves;
– It will lead to the emergence of new research areas in the development of various devices such as RF communication, sensor, medical ultrasound, filtering, waveguiding.

Author contribution statement

All Authors have contributed equally in the preparation of the manuscript.

References

1. S.A. Maier, Elastic, acoustic and seismic metamaterials, in *Handbook of Metamaterials and Plasmonics* (World Scientific Publishing Company, Singapore, 2017), Vol. 2
2. P.A. Deymier, *Acoustic Metamaterials and Phononic Crystals* (Springer, Heidelberg, 2013)
3. T.J. Cui, D.R. Smith, R. Liu, *Metamaterials: Theory, Design and Applications* (Springer, Heidelberg, 2010)
4. M.M. Sigalas, E.N. Economou, J. Sound Vib. **158**, 377 (1992)
5. H. Oraizi, S. Hedayati, IEEE Antennas Wirel. Propag. Lett. **10**, 67 (2011)
6. S. Tarafdar, A. Franz, C. Schulzky, K.H. Hoffmann, Physica A **292**, 1 (2001)
7. Z. Liu, X. Zhang, Y. Mao, Y.Y. Zhu, Z. Yang, C.T. Chan, P. Sheng, Science **289**, 1734 (2000)
8. A. Khelif, B. Djafari-Rouhani, V. Laude, M. Solal, J. Appl. Phys. **94**, 7944 (2003)
9. X. Li, Z. Liu, Solid State Commun. **133**, 397 (2005)
10. L.Y. Wu, L.W. Chen, C.M. Liu, Physica B **404**, 1766 (2009)

11. J.H. Oh, I.K. Lee, P.S. Ma, Y.Y. Kim, Appl. Phys. Lett. **99**, 083505 (2011)
12. I. El-Kady, R.H. Olsson, J.G. Fleming, Appl. Phys. Lett. **92**, 233504 (2008)
13. M. Lanoy, A. Bretagne, V. Leroy, A. Tourin, Crystals **8**, 195 (2018)
14. J. Wen, G. Wang, D. Yu, H. Zhao, Y. Liu, X. Wen, Sci. China Ser. E: Technol. Sci. **51**, 85 (2008)
15. N. Zen, T.A. Puurtinen, T.J. Isotalo, S. Chaudhuri, I.J. Maasilta, Nat. Commun. **5**, 3435 (2014)
16. W. Steurer, D. Sutter, J. Phys. D **40**, R229 (2007)
17. R.C. Norris, J.S. Hamel, P. Nadeau, J. Appl. Phys. **103**, 104908 (2008)
18. F. De Nicola, N.S.P. Purayil, D. Spirito, M. Miscuglio, F. Tantussi, A. Tomadin, F. De Angelis, M. Polini, R. Krahne, V. Pellegrini, ACS Photonics **5**, 2418 (2018)
19. N. Kuo, G. Piazza, Appl. Phys. Lett. **99**, 163501 (2011)
20. S. Castineira-Ibanez, C. Rubio, V. Romero-Garcia, J.V. Sanchez-Perez, L.M. Garcia-Raffi, Arch. Acoust. **37**, 455 (2012)
21. L. Xiao-Jian, F. You-Hua, Chin. Phys. B **22**, 036101 (2013)
22. S. Castiñeira-Ibáñez, C. Rubio, J. Redondo, J.V. Sánchez-Pérez, Appl. Phys. Express **7**, 042201 (2014)
23. K. Wang, Y. Liu, T. Liang, Physica B **498**, 33 (2016)
24. J. Huang, Z. Shi, W. Huang, Physica B **516**, 48 (2017)
25. K. Wang, Y. Liu, T. Liang, B. Wang, J. Phys. Chem. Solids **116**, 367 (2018)
26. B.B. Mandelbrot, *The Fractal Geometry of Nature* (World Scientific, Singapore, 1996)
27. T. Nakayama, K. Yakubo, *Fractal concepts in Condensed Matter Physics* (Springer, Heidelberg, 2003)
28. https://www.efunda.com/materials/materials_home/materials.cfm04.12.2019
29. F. Meseguer, M. Holgado, D. Caballero, N. Benaches, J. Sanchez-Dehesa, C. Lopez, J. Llinares, Phys. Rev. B **59**, 12169 (1999)
30. Y.F. Wang, Y.S. Wang, V. Laude, Phys. Rev. B **92**, 104110 (2015)
31. Y. Achaoui, T. Antonakakis, S. Brûlé, R.V. Craster, S. Enoch, S. Guenneau, New J. Phys. **19**, 063022 (2017)
32. R. Amuaku, W. Huabing, E.A. Asante, A. Buckman, Adv. Appl. Sci. **4**, 97 (2019)
33. F. Marcel, L. Molenkamp, *Topological insulators* (Elsevier Sci., Burlington, 2013)